Journal of Nuclear Materials 560 (2022) 153481

Contents lists available at ScienceDirect

Journal of Nuclear Materials

journal homepage: www.elsevier.com/locate/jnucmat

Coexistence of a self-interstitial atom with light impurities in a tungsten grain boundary

D. Fernández-Pello[a], M.A. Cerdeira[a], J. Suárez-Recio[a,b,c], R. González-Arrabal[b,c], R. Iglesias[a,*], C. González[d,e]

[a] Departamento de Física, Universidad de Oviedo, Oviedo E-33007, Spain
[b] Departamento de Ingeniería Energética, Instituto de Fusión Nuclear, Universidad Politécnica Madrid, Madrid E-28006, Spain
[c] Instituto de Fusión Nuclear "Guillermo Verlarde", Universidad Politécnica Madrid, Madrid E-28006, Spain
[d] Departamento de Física de Materiales, Universidad Complutense de Madrid, Madrid E-28040, Spain
[e] Instituto de Magnetismo Aplicado UCM-ADIF, Las Rozas, Madrid E-28230, Spain

ARTICLE INFO

Article history:
Received 23 July 2021
Revised 28 November 2021
Accepted 13 December 2021
Available online 22 December 2021

Keywords:
Metallic interfaces
Grain boundaries
Defects
Helium
Hydrogen
Formation energy
Migration energy
Ab-initio simulations
Density functional theory

ABSTRACT

In this paper, we report on ab initio simulations results focused on completing a thorough energetic, structural, charge and mobility analysis of the synergistic behaviour of diverse defects, namely self-interstitial atoms (SIA) and light impurity atoms (LIA), i.e., He and H, that would appear in W when simultaneously irradiated with the latter. In particular, the influence of a W⟨110⟩/W⟨112⟩ grain boundary (GB) in the behaviour of coexisting defects is studied and compared with the results obtained in the bulk. Four possible scenarios are analysed concerning the occupation of the GBs with: (i) a single SIA (ii) the simultaneous presence of two different defects, that is, He-H or SIA-LIA pairs, and (iii) the three types of defects together. The most stable configuration in each of these scenarios is detailed. Results show that GBs act as trapping sites for SIAs and LIAs and that the interaction between He and H is weak in all the analysed arrangements. They also indicate that the introduction of a SIA in a GB preloaded with He and H affects each of the atoms differently, as the former tends to stay close to the extra W atom, while the latter finds more comfortable accommodations away from the other two defects. In bulk W, the qualitative behaviour of He and H is quite similar and the presence of a LIA strongly affects the preferred orientation of the SIA dumbbell. Additionally, defect mobilities along the GB have been assessed concluding that the SIAs tend to move along the interfacial grooves, so to recombine with the vacancies present there.

1. Introduction

The ability to reduce light species (helium, hydrogen and its isotopes) accumulation in nuclear materials is crucial to improve their radiation tolerance by reducing the undesirable detrimental effects (blistering, exfoliation and/or cracking) which take place when these light species accumulate in the radiation-induced vacancies. One strategy to enhance radiation resistance consists in developing nanostructured materials [1–3]. The large grain boundary (GB) density favours the annihilation of interstitials and vacancies [4], promoting self-healing, which is the spontaneous return to the unirradiated structure, thereby improving resistence to radiation effects. However, self-healing of nanostructured materials takes place only under certain conditions, which are mainly related to the material properties (grain size and GB configuration and density) as well as to the irradiation conditions (e.g., fluence and temperature). Moreover, nanostructuring can also contribute to increase the radiation resistance of the material by creating effective diffusion channels through which light species can escape or by increasing the effective area for light species accumulation, so that blistering is delayed.

In this work the behaviour of diverse defect configurations in the W⟨110⟩/W⟨112⟩ GB created in agreement with the experimental evidence [5,6] is examined. This topic is very relevant since nanostructured W (NW) has been proposed as a potential alternative to coarse-grained W (CGW) as a plasma facing material (PFM) in nuclear fusion reactors [6–11] (and references therein). In those reactors, in both magnetic (MC) and inertial confinement (IC) ap-

* Corresponding author.
E-mail addresses: fernandezdario@uniovi.es (D. Fernández-Pello), ance@uniovi.es (M.A. Cerdeira), j.srecio@upm.es (J. Suárez-Recio), raquel.gonzalez.arrabal@upm.es (R. González-Arrabal), roberto@uniovi.es (R. Iglesias), cesar.gonzalez@ucm.es (C. González).

https://doi.org/10.1016/j.jnucmat.2021.153481

proaches, the PFM will be exposed simultaneously to large thermal loads and atomistic damage. Despite the differences in ion energies which depend on the confinement approach (below and above the displacement damage threshold for MC and IC, respectively) the arrival of light species (He and H) to the PFM leads to surface deterioration (blistering and fuzz formation in MC and blistering, cracking and exfoliation in IC), which seriously limit the lifetime of the material. Therefore, knowledge of the influence of GBs on the behaviour of He and H is crucial, in order to assess the capabilities and limitations of NW as a PFM.

Because of its importance, the influence of GBs on He and H retention has been extensively discussed. However, most of the studies performed to date have exclusively assessed the influence of the GBs on the behaviour of individual He and H. Furthermore, the majority of these works [12–15] have been performed at irradiation energies below the displacement damage threshold and just but a few have been devoted to examine the behaviour of He and H in W irradiated at energies above that threshold, whereby radiation-induced vacancies are created. Within the latter scenario, Object Kinetic MonteCarlo (OKMC) simulations devoted to analyse the influence of GBs on the density and distribution of vacancies at temperatures below (T = 473 K) and above (T = 573 K), the activation temperature for them to migrate [6,16] in samples predamaged with C at an energy of 665 keV, show that the vacancy concentration for the NW samples is notably higher than that for monocrystalline W. These results evidence that the GBs act as sinks for the (highly mobile) self-interstitial atoms (SIAs) generated during irradiation. Some complementary works have analysed the origin of the light species trapping inside the vacancies, as well as the maximum number of LIAs that the vacancies can accept [17–20].

Concerning the studies about the influence of GBs on the individual He and H atoms, all simulation and experimental data available show that both species have a great avidity to reach the GBs [21–31]. However, reported data about the influence of GBs on the behaviour of light species are not conclusive. Regarding H, some authors [29,32] report that its migration energy along the GB is larger than in the bulk whereas some others claim [6,16,33] that GBs behave as effective diffusion channels for H. The same holds for He migration along the GB [24,34,35]. In any case, either because the GBs favor the outdiffusion of light species or because they increase the surface area in which they can accumulate, GBs favour the formation of scarcely populated (H/V and He/V) clusters, a fact that may shift the threshold for detrimental effects to occur to larger fluences. Thus, in principle NW may exhibit a higher radiation resistance than CGW.

In order to evaluate the radiation response of NW as a PFM in nuclear fusion reactors, it is necessary to study its behaviour under mixed irradiation (He + H) [36]. Despite its importance, little work has been devoted to this topic, probably because of the reduced number of experimental facilities which can hardly mimic the harsh conditions (thermal loads and radiation damage) predicted to affect PFM in future nuclear fusion reactors [36,37]. In this context, computational simulations appear as a good tool to predict the behaviour of NW as a PFM. A reasonable number of potential materials can be selected by computational modelling, which thus positively contributes to accelerate the choice of the most effectively resilient and durable PFM [38,39]. To the best of our knowledge, so far all experimental and computational studies devoted to analyse the behaviour of W under mixed (He+H) irradiation have been performed in CGW but not in NW. In the following, the most relevant results carried out in CGW are summarised: Density Functional Theory (DFT) calculations show a strong attraction between He and H [29,40], indicating preferential trapping of H around HeV clusters. Molecular Dynamics (MD) simulations show that a large amount of hydrogen atoms can be accommodated around He bubbles [41], so that their mobility is consequently reduced [42], while increased retention was found experimentally [43]. Contrary to these findings, some other experiments studying the interaction of He and H with tungsten using He seeded deuterium (D) plasmas showed that He addition leads to reduced/supressed blistering [44–46], but promotes nanobubble formation in the near surface layer [47] which in turn fosters reduced D retention. While there have been several attempts to explain the reduced blistering and reduced D retention [48], the actual cause of these observations remains unclear, so that accurate DFT simulations can satisfactorily improve the knowledge on this very relevant topic.

From the above paragraphs, it appeared therefore obvious to us that the natural continuation of the above studies is to analyse the influence of GBs on the combined behaviour of He, H and SIAs. In this paper, DFT techniques have been used to investigate the behaviour of He and H impurity atoms simultaneously present at W GBs, combined or not with a preexisting SIA. The potential differences between both sides of the W⟨110⟩/W⟨112⟩ semicoherent interface have been specifically assessed. In parallel, we have also analysed the behaviour of coexistent He, H and SIAs in coarse grained (bulk) W, to fill in the existing gaps in the literature and be able to draw our own conclusions from setups we could always resort to via in-house simulations, and that were comparable to our own interfacial inputs. The similarities and differences between GB and bulk behaviour have been examined as well in what follows. Formation, binding, interaction and migration energies, as well as charge transfer and atomic volumes, have been computed in a variety of arrangements specially designed to shed light on the possible synergies arising from the coexistence of multiple kinds of point defects in the GB.

2. Methodology

DFT calculations were performed by means of the Vienna Ab initio Simulation Package (VASP) [49–51]. We have used the approximation developed by Perdew, Burke, and Ernzerhof (PBE) for the exchange and correlation functional [52], as well as the Projector Augmented Wave (PAW) pseudopotentials (PPs) provided by VASP [53]. The W PP included 6 electrons in the valence band (corresponding to the most usual configuration $5d^4 6s^2$). The H and He PPs were also characterised by their conventional $1s^1$ and $1s^2$ electronic configurations, respectively. Following the above prescriptions, we have estimated the lattice parameter of W to be 3.172 Å, close to the experimental value, namely 3.165 Å. The cutoff energy for the plane waves was fixed at 400 eV, except for the particularly demanding and precise calculations needed to find interaction energies (see below), where it was set to 479 eV. Relaxation was considered to be attained when the Hellmann–Feynman forces on the ions were no greater than 0.025 eV Angstrom^{-1}.

We have built a sufficiently large cubic bcc $5 \times 5 \times 5$ supercell (250 atoms) to represent the bulk system, as described elsewhere [18]. On the other hand, we formed a GB by adjoining two slabs each of 6 layers along the Z-axis, built in the W⟨110⟩ and W⟨112⟩ directions (the latter stretched by ~ 1 % in the X-direction due to the incoherent character of the interface), separated by a 12 Å vacuum, and extended on the XY plane as to be composed of 288 and 168 atoms, respectively, while the lateral size amounts up to 19.51 Å. The creation of this interface has been explained in detail in a previous work [19]. The atoms in the two last layers of the W⟨110⟩ slab and in the last one of the W⟨112⟩ have been fixed during relaxation in order to simulate the recovery of bulk-like conditions. In both bulk and GB structures, a single SIA, a single H atom and a single He atom have been implanted with the aim to understand the interactions and possible synergistic effects of having different combinations of defects in two distinct realistic

environments, namely, the ideal bulk and a semi-coherent W/W interface. The first Brillouin zone in the first case was sampled with a $4 \times 4 \times 4$ mesh, according to the Monkhorst-Pack grid sampling [54]. For the second structure we have used only the gamma point, as in previous works [19,35] we have shown that it suffices to capture the essential distinctive features of the interfacial system.

Moving on to the energetic calculations, the formation energy of a system $E_f(N_M, N_{SIA}, N_H, N_{He})$ containing N_M W atoms, N_{SIA} SIAs (in this work, N_{SIA} can be 0 or 1) and $N_{LIA} = N_H + N_{He}$ LIA atoms, where obviously N_H (N_{He}) stands for the number of H (He) atoms, can be easily estimated using the corresponding energies taken from the DFT simulations. Following the same recipe for the bulk case as in a previous work [55] and reforming in that spirit the prescriptions provided for other previous systems involving interfaces [19,35,56,57], we can define it as:

$$\begin{aligned} &E_f(N_M, N_{SIA}, N_H, N_{He}) \\ &\quad = E(N_M, N_{SIA}, N_H, N_{He}) - N_{SIA}E^{ref}(M) \\ &\qquad -N_H E^{ref}(H) - N_{He}E^{ref}(He) - E(N_M, 0, 0, 0), \end{aligned} \tag{1}$$

where the final energy obtained for the relaxed bulk or interfacial system is denoted by $E(N_M, N_{SIA}, N_H, N_{He})$ and $E(N_M, 0, 0, 0)$ is the initial case without defects. Finally, $E^{ref}(M)$, $E^{ref}(H)$, $E^{ref}(He)$ are the reference energies of the different elements present in the system, i.e., the metallic atoms (energy per atom) and the two possible species of LIAs. The reference energy of a metallic atom is obtained from a perfect crystal, considered to be the $5 \times 5 \times 5$ bcc supercell; the energy for the H atom is taken as half the energy of a H_2 molecule; and the energy of a He atom is obtained as the total energy of an isolated He inside an empty $5 \times 5 \times 5$ supercell, for coherency. With this general equation, the formation energy of a bulk SIA, i.e., 251 metallic atoms is given by $E_f(250, 1, 0, 0) = E(250, 1, 0, 0) - E^{ref}(M) - E(250, 0, 0, 0)$ and for a single interstitial LIA, e.g. H, $E_f(250, 0, 1, 0) = E(250, 0, 1, 0) - E(N_M, 0, 0, 0) - E^{ref}(H)$. The expressions for the SIA+H, SIA+He or SIA+H+He configurations are easily found likewise. A similar procedure may be followed for the 456 W atoms GB.

Analogously, the binding energy of the system is defined in terms of the formation energies of the system with the diverse objects close together and the system in which all those objects are far apart:

$$\begin{aligned} &E_b(N_M, N_{SIA}, N_H, N_{He}) \\ &\quad = N_{SIA}E_f(N_M, 1, 0, 0) + N_H E_f(N_M, 0, 1, 0) \\ &\qquad +N_{He}E_f(N_M, 0, 0, 1) - E_f(N_M, N_{SIA}, N_H, N_{He}), \end{aligned} \tag{2}$$

where the prescriptions given with regards to Eq. (1) are followed and a positive value means that the configuration is energetically favoured.

The interaction energy [55], E_i, can be defined for two arrangements. Firstly, when no SIA is present, by subtracting from the energy of the system with the H and He atom $E(M, H, He)$, the contributions of the impurity that is removed, say H (and analogously for He), $E(H)$, calculated inside the large empty supercell used for the total energy simulations and the contribution of the metallic atoms and the single He left $E(M, He)$. The latter is calculated by removing the H and constraining the metallic atoms to be fixed at the positions that are found from the relaxation of the structure when the H atom was still present. Thus, the equation that gives the H-metal interaction in this case is written as

$$E_i(M, H, He) = E(M, H, He) - E(H) - E(M, He). \tag{3}$$

Secondly, when a SIA is present as well, and if it is again the H atom that is removed, from the energy of the system, now $E(M, SIA, H, He)$, the $E(H)$ of the above paragraph and the contribution of the metallic atoms plus SIA and the He left $E(M, SIA, He)$ are subtracted. Analogous operations would be performed if only a He or both LIA are removed. Thus, the equation that gives the H-metal interaction in this case is written as

$$E_i(M, SIA, H, He) = E(M, SIA, H, He) - E(H) - E(M, SIA, He). \tag{4}$$

With this definition a positive value implies that the removal of the LIA is energetically favoured while a negative value means the opposite.

Subsequently, in order to further describe the electronic interactions taking place between the defects and the metallic matrices, the charge transfer and available atomic volumes for the former in the diverse configurations have been found by applying a Bader analysis [58], following the tools and prescriptions provided in Ref. [59] and references therein.

In a final step, we have analysed defect mobility in some selected cases, focused on assessing the mutual influence of the simultaneous presence of the various defects. The aim is to obtain the energy barriers required to displace the system from the most stable configurations found in the previous steps, following Transition State Theory (TST), as implemented in the Nudged Elastic Band (NEB) method [60,61] (and references therein) that can be applied within VASP. This methodology finds the path that minimises the energetic cost for a displacement from one initial to a final equilibrium configuration by following the most favourable trajectory (the one with the lowest migration barrier) to move between both states. The energy of the barrier is found by substracting the total energies at the saddle-point and at the initial configuration.

Table 1
Formation energies in eV for the different defects studied in this work (and other previous articles) at the W⟨110⟩/W⟨112⟩ GB and in the W bulk.

E_f (eV)	Interface	Bulk
H [19]	−0.09	0.96
He [35]	3.07	6.25
SIA	2.49	10.00
He + H	2.96	6.99
SIA + He	5.11	15.30
SIA + H	1.97	10.49
SIA + He + H	8.49	29.05

3. Results and discussion

3.1. One single defect: the self-interstitial case

Fig. 1 a shows the most stable SIA position (light-blue sphere) obtained from our simulations. For the sake of comparison, the most stable positions of the LIAs are shown in Fig. 1a and Fig. 1b for the interface and bulk, respectively. It is important to note that the SIA can find its preferential accommodation in a different groove far away from the most stable He and H sites. As He and H [19,35], the SIA presents a lower formation energy (see Table 1) at the interface, 2.49 eV, than in the bulk 10.00 eV, which means that it will tend to move from the bulk to the interface, most favourably as the migration energies are low. This value was calculated within a $5 \times 5 \times 5$ cubic unit cell (see the Methodology section for details) and it is in good agreement with the data presented in previous works [55,62,63]. In all of them, the most stable SIA structure was obtained for the dumbbell (111), denoted from now on as d111, meaning that the W atom at the centre of the cube is doubled following a crystallographic (111) direction as shown in Fig. 1b. The great difference between the two values of the formation energy suggests that the W atoms, out of their bulk positions, will tend to move until they can find a certain GB, interface or surface. This behaviour is similar to that of both LIAs

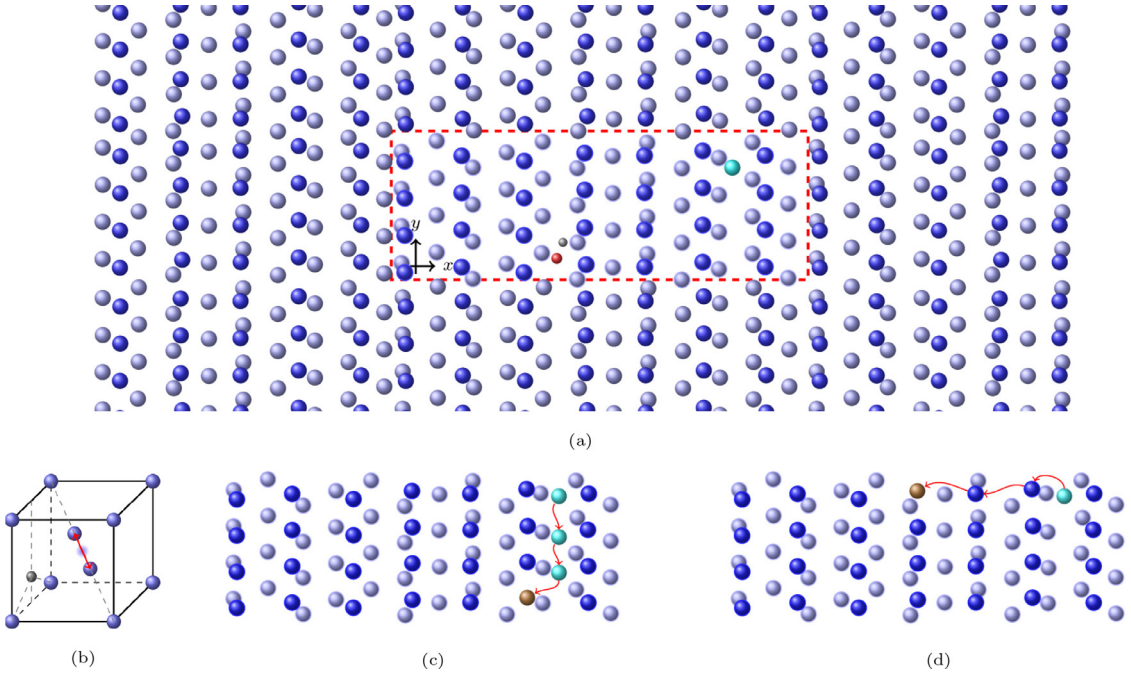

Fig. 1. (a) Frontal view of the W ⟨110⟩/W⟨112⟩ GB including H, He and SIA in their corresponding most stable sites for each defect alone. (b) bcc cell containig a tetrahedral LIA and a dumbbell along the ⟨111⟩ direction, as shown by the red arrow. (c) and (d) Diverse possible migration pathways of a SIA towards a hypothetical vacancy.

as mentioned above. We would like to stress as an additional coincident feature that the extra W atom is positioned closer to the ⟨112⟩ surface than to the ⟨110⟩ one. On the contrary, it is important to note that this position is far away from the most stable sites of both the He and H atoms.

We have studied the behaviour of a SIA when it is close to a vacancy. For that purpose, we have created a vacancy far away from the extra W atom but in the same groove (Fig. 1c) and in the most stable site at the interface (Fig. 1d). In both cases, the vacancy is labelled by a brown circle. At this distant position, the structure with a SIA and a vacancy is stable after relaxation, but the system has an energy 3.23 eV larger than that of the interface without defects, certainly more stable than any other arrangement presenting both vacancies and SIA. It is expected and highly desirable that the extra W atom can move easily to occupy the empty space provided by the vacancy, since this is required for the material to self-heal. We have tried to rationalise this process by doing different migration calculations where the W atom jumps from quasi-equivalent SIA positions until it finally reaches the vacancy site (see the sketch depicted in Fig. 1c). In a first step, the energy barrier is estimated to be 1.6 eV by using the NEB method (see the section devoted to Methodology for more details). Such a high value suggests that this particular motion will be hampered in this direction. Only when the SIA atom is close to the vacancy, the W atom will move very easily to fill in the vacancy. The energy barrier in this second case has been found to be 0.04 eV. Given such a small value, we claim that the SIA atoms will tend to occupy only the vacancies present in their close neighbourhood at the interface.

We have tried an alternative mechanism depicted in Fig. 1d). It should be noted that the selected vacancy is not placed in the most favourable site, since the energy of the system is 0.13 eV larger if the vacancy was sitting at this position [35]. For that reason, we have performed the calculation with the SIA and the vacancy in their corresponding more favourable sites, trying to displace the extra atom along a direction perpendicular to the grooves formed by the W⟨112⟩ surface (see the sketch depicted in Fig. 1d). Even though this suggested migration mechanism could be thought as a process with a high energy cost, we have found a completely different result. When the initial SIA atom starts to move along the X-direction, it pushes the atoms in the W⟨112⟩ rows leading to an atomic rearrangement that finally fills in the vacancy with a nearby atom. This process is reminiscent of the motion of a SIA in the bulk where a true individual atomic displacement does not occur. Instead, a concatenation of short movements along the ⟨111⟩ direction takes place, leading to a collective defect usually called "crowdion". Similarly to the case in the bulk, we obtained a very small barrier for such a process at the interface, namely, only 0.03 eV. This value is larger than the one obtained at the bulk, i.e., around 0.01 eV [63], but it is still much smaller than the motion proceeding along the groove, suggesting that this mechanism will be preferentially followed by the system to fill in the vacancies at the interface, reducing their number there. Even though the migration barrier is very small, in principle allowing its migration back to the bulk, it is expected that the defect could return to the GB, since the formation energy of the SIA is much lower at the interface than in the bulk.

In summary, from the two mechanisms discussed in the above paragraphs, the one shown in Fig. 1d) is energetically much more favourable and, even if it appears to be more complicated, would definitely be the one followed by the SIA to fill in the vacancy present at the GB.

3.2. Simultaneous presence of He and H at the GB

In a second step, we have combined both types of LIAs, i.e., the H and He atoms at the selected W⟨110⟩/W⟨112⟩ interface. As mentioned before, a single He or H atom prefers to sit at the most convenient sites provided by their immediate surroundings. More precisely, He tries to find as wide as possible hollow geometries, while H attempts to form bonds to one of the nearest metallic atoms in order to minimise the deformation of the system (see Fig. 1a). When we put both atoms together, they find a better accommodation by occupying, approximately, their corresponding most stable position but at different unit cells along the Y-direction. More-

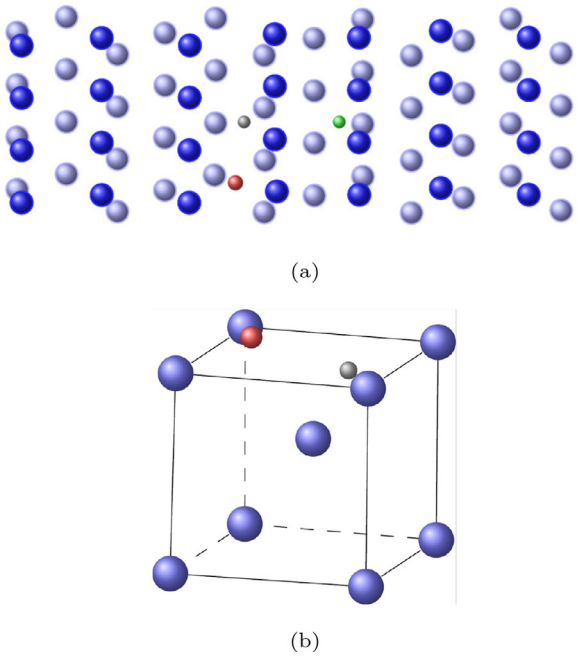

Fig. 2. (a) Frontal view of the most stable structures for a He atom ● and a H atom, ● in the W ⟨110⟩●/W⟨112⟩● GB (the ● corresponds to a H atom in a different groove) and (b) the corresponding case in the bulk.

Table 2
Distances between pairs of defects in different configurations at the interface and in the bulk.

distance (Å)		Interface	Bulk
He + H		3.23	1.68
SIA + He		2.89	2.09
SIA + H		14.03	2.03
SIA	SIA, He	2.89	2.39
+	SIA, H	14.04	1.92
He	He, H	13.17	1.77
+			
H			

over, as happened with the single defects, both He and H stay close to the W⟨112⟩ surface in the groove formed by the parallel W rows [19,35]. Fig. 2a depicts this structure, where the red (grey) sphere represents the He (H) atom. The distance between both atoms is 3.23 Å (see Table 2), slightly larger than the distance between two consecutive W atoms in the Y-direction, namely 2.75 Å. Several plausible arrangements have been assessed in an effort to find the most stable configuration. We have attempted to force the H and He atoms to stay closer within the very same unit cell in the Y-direction, but the resulting structure leads to a 0.29 eV less stable configuration than the one shown in Fig. 2a. Subsequently, the H atom has been displaced two unit cells along the Y-direction, leading to a structure less stable by 0.10 eV. Interestingly, this energy difference is similar to the one obtained when the H atom was displaced to its second most stable position at a different groove in the GB (0.13 eV [19]), as shown in Fig. 2a (green sphere). This result suggests that He and H prefer to remain close to each other at a distance of about one unit cell in the Y-direction, but their mutual influence decreases very fast with increasing distance between them. This effect is reflected in the migration energy obtained for the H approaching process to the most stable site. Its value was estimated to be 0.11 eV, very close to the 0.12 eV obtained for the energy barrier of one single atom moving along the same groove [19].

The formation energies obtained for the most stable cases for a single LIA are 3.07 eV for He and -0.09 eV for H, see Table 1. In turn, the calculated formation energy associated to the most stable geometry when both LIAs are simultaneously present takes a value of 2.96 eV. It should be noted that the latter number is almost the addition of the former two, which indicates the hardly appreciable interaction between both LIAs.

We have also analysed the cases with either one of the atoms in the second layer. Both types of LIAs present a similar behaviour to the single atom case, i.e., when we studied individually the behaviour of either He or H in the vicinity of the interface [19,35]. In these previous works, we obtained that the He atom tends to move directly to the interface from the second layer on both surfaces, W⟨110⟩ and W⟨112⟩, while the H atom finds a metastable position on the W⟨110⟩ side with a formation energy of 0.87 eV, higher (i.e., less stable) than the configuration with the H atom at the interface.

Considering now the situation with both LIAs simultaneously present at the GB, the inclusion of one H atom at the interface also allows the He atom to find a metastable accommodation on the second layer of the W⟨110⟩ surface as well, but in this case it has an energy of 2.71 eV, higher than the configuration with both atoms at the interface. As in the cases with a single LIA, the H atom finds metastable sites in the second layer of the W⟨110⟩ surface revealing a dependence on the distance between both LIAs. When the H is placed at a unit cell distance along the Y-direction in the second layer of the W⟨110⟩, the energy found is 0.86 eV higher than the most stable arrangement, i.e., with both LIAs at the interface. It should be noted that this value is very close to the one obtained for a single H atom [19]. These results evidence the low influence that the simultaneous presence of both LIAs has on the final reconstruction of the GB when their mutual distance is large enough.

Furthermore, we have estimated the energy cost for the movement of one He or H atom to the interface in the aforementioned structures. Firstly, in the case of a He at the second layer, the energy barrier is found to be 0.05 eV, lower than the value obtained in the bulk, namely, 0.08 eV [17]. Secondly, the H atom can move to the interface from the second layer overcoming a barrier of 0.15 eV, i.e., a value larger than that for the He atom but again lower than in the bulk (0.21 eV) [19]. Interestingly, this value is the same than that for a single H atom [19], confirming the low He-H interaction when both atoms are at a sufficient distance from each other.

In order to compare to the bulk case, we have performed the same calculation within a $5 \times 5 \times 5$ unit cell. As both He and H atoms find the most stable configuration at a tetrahedral site, we have started the calculation with both atoms in close positions on the same XY plane. We can obtain a slightly more stable structure by displacing the atoms along the opposite direction along the Z-axis. This effect can be observed in Fig. 2b where the He atom is displaced upwards 0.37 Å while the H atom is only shifted asymmetrically 0.06 Å downwards, leading to a He-H distance of 1.68 Å, a much lower value than the one obtained at the interface, namely, 3.23 Å (see Table 2). As shown in Table 1, the formation energy of such a structure is 6.99 eV, much larger than the value at the interface (2.96 eV). This value is even larger than that for the case with a single LIA at the second layer of the W⟨110⟩ surface, thus showing the great attraction exerted by the interface on both LIAs. Similarly to the interface, the formation energy when the two LIAs are close to each other in their most stable positions in the bulk decreases as well. However, such a reduction is much higher in the bulk than at the interface, being only 0.02 eV for the latter (2.96 eV vs the addition of 3.07 eV and -0.09 eV for the single He and H, respectively) while for the former it is 6.99 eV vs the addition of 6.25 eV and 0.96 eV for the single He and H, respectively. This difference may be explained by the larger mutual distance between the He and the H at the interface. In fact, as we separate the H to another unit cell in the bulk, the energy increases, becoming

Table 3
Interaction energy in eV for the different defects studied in the present work at the interface (GB) and in the bulk.

E_i (eV)	GB	bulk
M+He+H - H	-0.40	0.74
M+He+H - He	2.51	4.83
M+SIA+He+H - He - H	2.54	4.76
M+SIA+He+H - H	-0.12	0.54
M+SIA+He+H - He	2.66	4.36

Table 4
Charge and atomic volume (At Vol) results of the Bader analysis in the presence of LIA and SIA in the interface (GB) and bulk.

Case	**Charge** (e)		**At Vol** (Å^3)	
	GB	bulk	GB	bulk
H	1.35	1.50	4.00	3.20
He	2.12	2.19	3.94	3.29
He+H	2.12	2.17	4.05	3.27
	1.35	1.46	4.10	3.32
SIA	6.20	6.27	15.69	15.41
SIA+H	6.20	6.20	15.68	14.92
	1.34	1.40	4.02	3.21
SIA+He	6.21	6.26	15.72	15.25
	2.12	2.16	4.07	3.36
SIA+He+H	6.21	6.13	15.72	14.80
	2.12	2.15	4.06	3.36
	1.34	1.43	4.02	3.26

0.09 eV (0.19 eV) for the nearest (next-nearest) unit cells. Thus, the preferential accommodation of both LIAs lies within the same unit cell. This seems to be in contradiction with the case at the interface, where they rather stay separated in different unit cells, adjacent along the Y-direction. In order to justify this apparent discrepancy, we propose again that the H atom can easily find a more energetically favourable bulk environment among the W atoms that surround a previously present He atom, while at the interface a similar advantageous site may be found by the H atom somewhat farther away from the He atom, in a neighbouring unit cell.

The binding energy between H and He found in the bulk by using Eq. (2) is 0.22 eV, in agreement with Ref. [63] (0.2 eV), i. e., there is a slight attraction between H and He in that case. At the interface, the binding energy is even smaller, namely, 0.02 eV, which is not surprising, given that H and He tend to be far from each other.

At the two top rows of Table 3, the interaction energies found from Eq. (3) are presented. Recalling the discussion thereby given, for both GB and bulk the removal of the He atom is energetically more costly than the removal of the H or, in other words, the interaction of He within the metallic matrix in the presence of a H atom is highly repulsive, while the interaction of H in the presence of a He is only slightly repulsive (attractive) in the bulk (GB). This is in agreement with the findings of Ref. [55] for a single LIA in the metallic matrix, where the authors used a different plane-wave code.

Table 4 shows the results of the Bader analysis performed when H and He are simultaneously present in the bulk and at the interface, together with the charges and atomic volumes of the individual LIA for comparison. It is obvious that more charge is transferred to both LIA when they are sitting at bulk positions, i.e., bonding should be stronger. However, the simultaneous presence of both H and He in the bulk (at the GB) slightly reduces (increases) the charge of each LIA. Concerning the atomic volumes, they are increased when both LIA are present, and as could be expected, they are much greater at the interface than in the bulk, thereby facilitating their accommodation at the GB.

3.3. Two types of defects: SIA and LIA

In this subsection, the simultaneous presence of a single SIA and a single LIA is analysed. The starting arrangement combines the most stable sites for both types of atoms. After relaxation, two different behaviours dependent on the type of LIA are evidenced:

(a) H finds the best accommodation in the position shown in Fig. 3a. Thus, hydrogen seems to ignore the electronic environment created by the extra W atom to stay close to its most stable place at the interface. As shown in Table 1, the formation energy of this configuration is 1.97 eV. When we tried to bring the H atom closer to the SIA, the formation energy increased up to 2.43 eV, notably higher than for the two separated defects.
(b) On the contrary, as shown in Fig. 3b, the He atom prefers to sit close to the SIA. The He atom takes advantage of the deformation created by the SIA and, despite it remains in the same groove, it is displaced one unit cell in the Y-direction. In this situation, the SIA creates new open space that leads to a reduction in the repulsion exerted by the areas with high electronic density on the He atom [18,31,35]. This in turn favours a lower energy cost due to the deformation of the structure. The configuration shown in Fig. 3b presents a formation energy of 5.11 eV. From Table 1, the latter value is 0.45 eV more stable than the situation with the individual SIA and He atoms placed in their corresponding most stable sites shown in Fig. 1a.

Fig. 3 c and 3 d shows the same combination of defects in the bulk for a SIA with a H/He atom, respectively. The LIA is placed in the same cubic unit cell as the SIA. In both cases, the dumbbell that prior to relaxation lies along the (111) direction is apparently displaced to the (110) direction, showing the strong effect of the LIAs on the SIA orientation. The formation energies for both structures are much larger than for the corresponding cases at the interface, namely, 10.49 eV and 15.30 eV for the H and the He, respectively. The very large difference obtained confirms the great tendency of the defects to move and accumulate at the GB. Interestingly, as we move the LIA atom one unit cell away from the SIA, the formation energy of the system increases up to 10.78 eV (16.25 eV) for a H (He) atom, implying that in the bulk the closer the LIAs are to the SIA, the more stable is the configuration, while at the interface, at least, the H atoms can remain at distant positions.

The binding energy between SIA and H in the bulk from Eq. (2) is 0.47 eV, much higher than in previous DFT calculations (0.33 eV in Ref. [63,64] and 0.27 eV in [65]), which were performed under less demanding conditions than ours. At the interface, the corresponding result is 0.43 eV, which means a little change, but is somewhat reduced due again to the substantial separation between SIA and H. In turn, the binding energy between SIA and He in the bulk, again from Eq. (2) is 0.95 eV, that compares extremely favourably to the value in Ref. [63], namely, 0.94 eV, while at the interface it takes on a value of 0.45 eV. This is another indication of the attractive behaviour of the SIA and He, in opposition to what happens for H.

Regarding the Bader analysis of the defect configurations presented in this section, the general trends are the same as in the preceding section, as shown in Table 4, since both SIA and LIA acquire more charge in the bulk than at the GB and the available atomic volumes are always higher at the interface. The most noticeable difference is that the charge of the SIA is essentially the same in the presence of both LIA and also the same as when the SIA is alone. Moreover, the charge of the SIA in the SIA+H configuration is identical for bulk and GB.

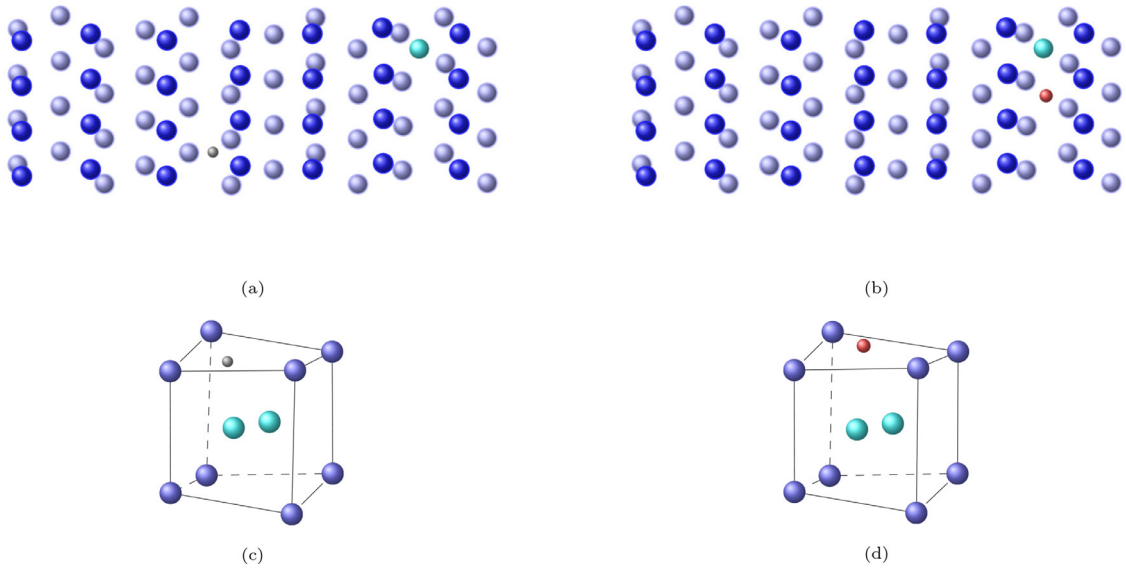

Fig. 3. Frontal view of the most stable structure for a H atom ● (a) and a He atom ● (b) with a SIA● in the GB; (c) and (d) show the same for the bulk.

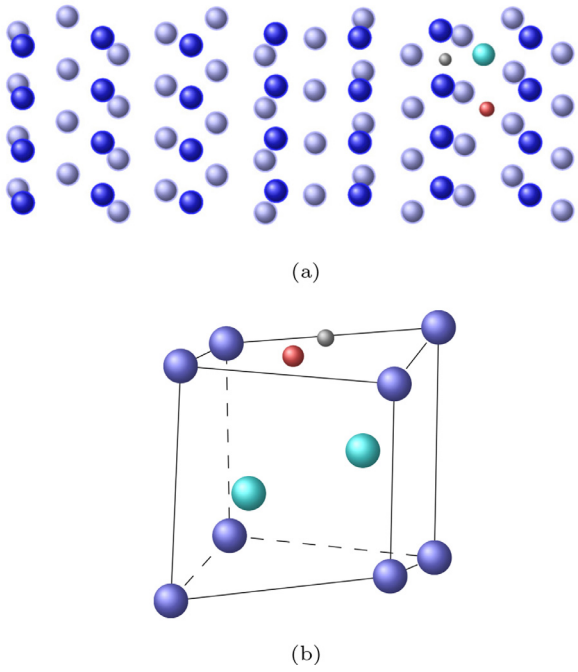

Fig. 4. Frontal view of the most stable structure for a H atom ●, He atom ● and SIA● in (a) a W ⟨110⟩●/W⟨112⟩● GB and (b) in the bulk.

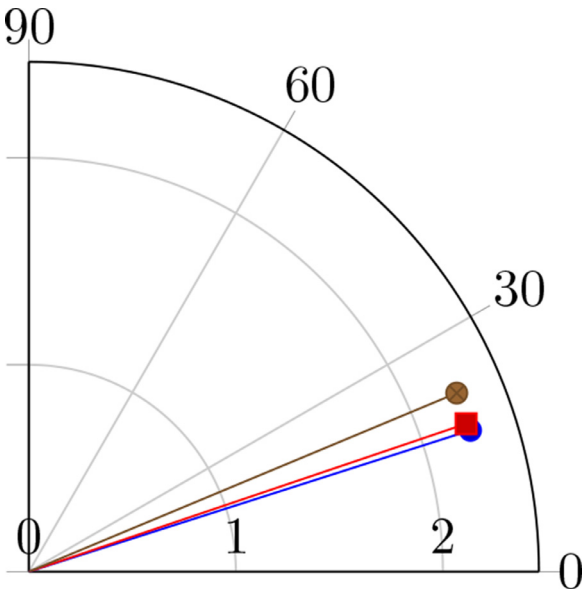

Fig. 5. Angle of rotation, in degrees, of the SIA with respect to the theoretical (111) direction for the three groups of bulk defects studied: SIA + H (●), SIA+He (●), SIA+He+H (■).

3.4. All three defects together: SIA, He and H

In the following, we analyse the coexistence of the three types of defects, i.e., we insert together in the same unit cell one SIA, one He atom and one H atom. From our previous calculations, the H atom prefers to be far away from the SIA (see Fig. 3a), while the He atom finds a better accommodation closer to the extra W atom (see Fig. 3b). Consequently, a combination of the more stable structures corresponding to the SIA and H case, on the one hand, and the SIA and He case, on the other, can be a good choice to define the initial arrangement. This structure, depicted in Fig. 4a resulted to be the most stable one. For the sake of comparison, when we tried to adjoin the H atom to the SIA-He group, an alternative less stable structure was found by an energy difference of more than 0.10 eV.

As happened with all the cases analysed previously, the formation energy of the configuration of a SIA with one He atom and one H atom has a much lower value as compared to the same case in the bulk. In Table 1 a huge difference can be found, namely 8.49 eV at the interface versus 29.05 eV in the bulk. Fig. 4b shows the structure with the He and H atoms placed in a position close to the one shown in Fig. 2b. It is apparent that the final reconstruction affects basically the SIA, since the two W atoms that form the dumbbell (111) end up being slightly rotated. This closely resembles the situation for one single LIA close to the SIA as mentioned before. Specifically, the angles of rotation with respect to the bulk (111) direction for the three different defect arrangements containing a SIA are shown in Fig. 5. As expected, the deviation increases from the configuration with a single H (17.76°) to that with a single

He (18.70°) being the largest (22.67°) when both LIAs are simultaneously present.

It is important to mention that the calculations performed when introducing a SIA in the bulk were done in order to compare to the process taking place at the GBs. However, this may not reproduce the real case in samples with a large density of GBs since, if we consider the large differences between the migration energies of vacancies and interstitials in W, we expect interstitials to quickly migrate toward GBs where they are trapped, whereas vacancies remain in the interior of the grain. In this frame, a much more realistic situation would be to consider that only vacancies remain in the bulk. DFT calculations performed by several authors under the latter situation illustrate that both He and H are largely attracted by the vacancies [66–68]. Moreover, if He, H and vacancies coexist in the bulk, He and vacancy complexes can act as additional trapping sites for H [40,69].

At the three bottom rows of Table 3, the interaction energies found from Eq. (4) are shown. Again, for both GB and bulk the interaction of He with a SIA and a H atom is highly repulsive, while the interaction of H with a SIA and a He atom is only slightly repulsive (attractive) in the bulk (GB). If the interaction of coexisting He and H with the metallic matrix in the presence of a SIA is considered, the energies obtained may be approximated by the added contribution of the interactions of the two individual defects. Let us highlight again that the interaction energies for H change sign from the bulk to the GB, thus confirming the affinity of hydrogen for the latter.

The Bader analysis for this particular case shows a very significant change with regards to the two previously assessed configurations, i.e., the charge transfer to the SIA from its environment is smaller in the bulk than at the interface. This could be an indication of the combined synergistic effect of both LIA at the GB that eventually may give rise to a reduced mobility in the SIA and hinder its affinity to fill in the vacancies present there. Further computations would be needed to confirm or dismiss this point. It is interesting to highlight that the charge transfer and available volumes for the three coexisting defects at the interface are almost identical to the dual arrangements discussed in the previous section, while they show some differences in the bulk.

4. Conclusions

We have performed a deep systematic analysis of the behaviour of different kinds of defects coexisting in a W $\langle 110\rangle/\langle 112\rangle$ interface. We have found that all of them present a clear tendency to move to the interfaces due to the lower formation and attractive interaction energies obtained as compared to their corresponding counterpart in the W-bulk, in agreement with the larger charge transfer and available atomic volumes in the former system. Our results show an easy procedure for extra W atoms at the GB to occupy the vacancies, suggesting that the number of vacancies at the interface may be low. Interestingly, when a LIA and a SIA are simultaneously present, the behaviour of the two types of LIA is remarkably different: H finds favourable environments to form bonds and in so doing ignores the SIA whereas He prefers to stay close to the SIA within the same unit cell. Furthermore, when the three defects are present at the GB, the observed reconstruction basically affects the SIA. In this situation, H prefers to stay in its isolated more stable site, far away from the SIA+He pair showing its little affinity to interact with both the SIA and the He. On the contrary, in the bulk, the three defects could appear at the same unit cell, leading to a strong rearrangement in the (111) orientation of the original dumbbell.

The simultaneous presence of the three point defects analysed in a W GB points out to the fact that the avidity of the SIA to occupy the nearest vacancy available may be obstructed by the simultaneous presence of helium, while that of hydrogen does not imply any appreciable hindrance to that tendency. Such a behaviour of the He atoms is very relevant, at temperatures at which the vacancy motion is already activated, because of two reasons. On the one hand, it could hamper the vacancy-SIA recombination process at the GB which would prevent the self-healing effect. On the other hand, if the affinity of the He atom for the vacancy at the interface is larger than that shown for the SIA, the He atom would rather stay inside the vacancy and thus, when the number of He atoms is large enough, would produce grain boundary decohesion. Further research is needed in order to elucidate this point.

Declaration of Competing Interest

The authors declare that they have no known competing financial interests or personal relationships that could have appeared to influence the work reported in this paper.

CRediT authorship contribution statement

D. Fernández-Pello: Data curation, Formal analysis, Investigation, Writing – review & editing. **M.A. Cerdeira:** Data curation, Formal analysis, Investigation, Writing – review & editing. **J. Suárez-Recio:** Formal analysis, Writing – review & editing. **R. González-Arrabal:** Formal analysis, Funding acquisition, Investigation, Project administration, Resources, Supervision, Writing – original draft, Writing – review & editing. **R. Iglesias:** Formal analysis, Funding acquisition, Investigation, Methodology, Project administration, Resources, Supervision, Writing – original draft, Writing – review & editing. **C. González:** Formal analysis, Investigation, Methodology, Resources, Supervision, Writing – original draft, Writing – review & editing.

Acknowledgment

The authors would like to gratefully acknowledge Angel Gutiérrez at the UNIOVI Scientific Computation Centre (C3) for his technical help and CPU time.

This research was funded by the Spanish Ministry of Science and Innovation, through the project RADIAFUS V, grant number PID2019-105325RB-C32, and network ROSALES, grant number RED2018-102616-T, by the Community of Madrid through the project NanomagCOST-CM, grant number S2018/NMT-4321 and by the Multi-year Agreement with the Polytechnic University of Madrid in the line of action Excellence Program for University Teaching Staff. The computational resources were provided by the Spanish Supercomputing Network (RES) (projects QCM-2018-3-0001 and QCM-2019-1-0002) resource Caléndula based at the FC-SCL, León, Spain and CAESARAUGUSTA based on Zaragoza, Spain.

References

[1] G. Ackland, Controlling radiation damage, Science 327 (5973) (2010) 1587–1588, doi:10.1126/science.1188088.
[2] X.M. Bai, A.F. Voter, R.G. Hoagland, M. Nastasi, B.P. Uberuaga, Efficient annealing of radiation damage near grain boundaries via interstitial emission, Science 327 (5973) (2010) 1631–1634, doi:10.1126/science.1183723.
[3] X. Zhang, K. Hattar, Y. Chen, L. Shao, J. Li, C. Sun, K. Yu, N. Li, M.L. Taheri, H. Wang, J. Wang, M. Nastasi, Radiation damage in nanostructured materials, Prog. Mater. Sci. 96 (2018) 217–321, doi:10.1016/j.pmatsci.2018.03.002.
[4] I.J. Beyerlein, M.J. Demkowicz, A. Misra, B.P. Uberuaga, Defect-interface interactions, Prog. Mater. Sci. 74 (2015) 125–210, doi:10.1016/j.pmatsci.2015.02.001.
[5] N. Gordillo, M. Panizo-Laiz, E. Tejado, I. Fernandez-Martinez, A. Rivera, J.Y. Pastor, C.G. de Castro, J. del Rio, J.M. Perlado, R. Gonzalez-Arrabal, Morphological and microstructural characterization of nanostructured pure α-phase W coatings on a wide thickness range, Appl. Surf. Sci. 316 (2014) 1–8, doi:10.1016/j.apsusc.2014.07.061.
[6] G. Valles, M. Panizo-Laiz, C. González, I. Martin-Bragado, R. González-Arrabal, N. Gordillo, R. Iglesias, C.L. Guerrero, J.M. Perlado, A. Rivera, Influence of grain boundaries on the radiation-induced defects and hydrogen in nanostructured

and coarse-grained tungsten, Acta Mater. 122 (2017) 277–286, doi:10.1016/j.actamat.2016.10.007.
[7] R. Gonzalez-Arrabal, M. Panizo-Laiz, N. Gordillo, E. Tejado, F. Munnik, A. Rivera, J.M. Perlado, Hydrogen accumulation in nanostructured as compared to the coarse-grained tungsten, J. Nucl. Mater. 453 (1–3) (2014) 287–295, doi:10.1016/j.jnucmat.2014.06.057.
[8] V.A. Ksenofontov, T.I. Mazilova, E.V. Sadanov, O.V. Dudka, A.A. Mazilov, I.V. Starchenko, I.M. Mikhailovskij, Helium induced reduction of the grain-boundary tensile strength in tungsten, J. Nucl. Energy Sci. Power Gener. Technol. 3 (2014) 2.
[9] G. Valles, C. González, I. Martin-Bragado, R. Iglesias, J.M. Perlado, A. Rivera, The influence of high grain boundary density on helium retention in tungsten, J. Nucl. Mater. 457 (2015) 80–87, doi:10.1016/j.jnucmat.2014.10.038.
[10] Z. Chen, L.L. Niu, Z. Wang, L. Tian, L. Kecskes, K. Zhu, Q. Wei, A comparative study on the in situ helium irradiation behavior of tungsten: coarse grain vs. nanocrystalline grain, Acta Mater. 147 (2018) 100–112, doi:10.1016/j.actamat.2018.01.015.
[11] O. El-Atwani, E. Martinez, E. Esquivel, M. Efe, C. Taylor, Y.Q. Wang, B.P. Uberuaga, S.A. Maloy, Does sink efficiency unequivocally characterize how grain boundaries impact radiation damage? Phys. Rev. Mater. 2 (11) (2018) 113604, doi:10.1103/physrevmaterials.2.113604.
[12] Y. Ueda, T. Funabiki, T. Shimada, K. Fukumoto, H. Kurishita, M. Nishikawa, Hydrogen blister formation and cracking behavior for various tungsten materials, J. Nucl. Mater. 337–339 (2005) 1010–1014, doi:10.1016/j.jnucmat.2004.10.077. PSI-16, URL https://www.sciencedirect.com/science/article/pii/S0022311504008475
[13] T.J. Petty, M.J. Baldwin, M.I. Hasan, R.P. Doerner, J.W. Bradley, Tungsten 'fuzz' growth re-examined: the dependence on ion fluence in non-erosive and erosive helium plasma, Nucl. Fusion 55 (9) (2015) 093033, doi:10.1088/0029-5515/55/9/093033.
[14] O.V. Ogorodnikova, Fundamental aspects of deuterium retention in tungsten at high flux plasma exposure, J. Appl. Phys. 118 (7) (2015) 074902, doi:10.1063/1.4928407.
[15] L. Gao, A. Manhard, W. Jacob, U. von Toussaint, M. Balden, K. Schmid, High-flux hydrogen irradiation-induced cracking of tungsten reproduced by low-flux plasma exposure, Nucl. Fusion 59 (5) (2019) 056023, doi:10.1088/1741-4326/ab0915.
[16] M. Panizo-Laiz, P. Díaz-Rodríguez, A. Rivera, G. Valles, I. Martín-Bragado, J.M. Perlado, F. Munnik, R. González-Arrabal, Experimental and computational studies of the influence of grain boundaries and temperature on the radiation-induced damage and hydrogen behavior in tungsten, Nucl. Fusion 59 (8) (2019) 086055, doi:10.1088/1741-4326/ab26e9.
[17] C. González, R. Iglesias, Migration mechanisms of helium in copper and tungsten, J. Mater. Sci. 49 (23) (2014) 8127–8139, doi:10.1007/s10853-014-8522-7.
[18] C. González, M.A. Cerdeira, S.L. Palacios, R. Iglesias, Reduction of the repulsive interaction as origin of helium trapping inside a monovacancy in BCC metals, J. Mater. Sci. 50 (10) (2015) 3727–3739, doi:10.1007/s10853-015-8935-y.
[19] C. González, M. Panizo-Laiz, N. Gordillo, C.L. Guerrero, E. Tejado, F. Munnik, P. Piaggi, E. Bringa, R. Iglesias, J.M. Perlado, R. González-Arrabal, H trapping and mobility in nanostructured tungsten grain boundaries: a combined experimental and theoretical approach, Nucl. Fusion 55 (11) (2015) 113009, doi:10.1088/0029-5515/55/11/113009.
[20] C. Guerrero, C. González, R. Iglesias, J.M. Perlado, R. González-Arrabal, First principles study of the behavior of hydrogen atoms in a W monovacancy, J. Mater. Sci. 52 (2016) 1445–1455, doi:10.1007/s10853-015-9464-4.
[21] F. Sefta, K.D. Hammond, N. Juslin, B.D. Wirth, Tungsten surface evolution by helium bubble nucleation, growth and rupture, Nucl. Fusion 53 (7) (2013) 073015, doi:10.1088/0029-5515/53/7/073015.
[22] L. Hu, K.D. Hammond, B.D. Wirth, D. Maroudas, Interactions of mobile helium clusters with surfaces and grain boundaries of plasma-exposed tungsten, J. Appl. Phys. 115 (17) (2014) 173512, doi:10.1063/1.4874675.
[23] Z. Chen, L.J. Kecskes, K. Zhu, Q. Wei, Atomistic simulations of the effect of embedded hydrogen and helium on the tensile properties of monocrystalline and nanocrystalline tungsten, J. Nucl. Mater. 481 (2016) 190–200, doi:10.1016/j.jnucmat.2016.09.024.
[24] X.-X. Wang, L.-L. Niu, S. Wang, Strong trapping and slow diffusion of helium in a tungsten grain boundary, J. Nucl. Mater. 487 (2017) 158–166, doi:10.1016/j.jnucmat.2017.02.010.
[25] G. Nandipati, W. Setyawan, H.L. Heinisch, K.J. Roche, R.J. Kurtz, B.D. Wirth, Displacement cascades and defect annealing in tungsten, part II: object kinetic monte carlo simulation of tungsten cascade aging, J. Nucl. Mater. 462 (2015) 338–344, doi:10.1016/j.jnucmat.2014.09.067.
[26] A.M. Ito, A. Takayama, Y. Oda, T. Tamura, R. Kobayashi, T. Hattori, S. Ogata, N. Ohno, S. Kajita, M. Yajima, Y. Noiri, Y. Yoshimoto, S. Saito, S. Takamura, T. Murashima, M. Miyamoto, H. Nakamura, Molecular dynamics and Monte Carlo hybrid simulation for fuzzy tungsten nanostructure formation, Nucl. Fusion 55 (7) (2015) 073013, doi:10.1088/0029-5515/55/7/073013.
[27] T. Oda, D. Zhu, Y. Watanabe, Kinetic Monte Carlo simulation on influence of vacancy on hydrogen diffusivity in tungsten, J. Nucl. Mater. 467 (2015) 439–447, doi:10.1016/j.jnucmat.2015.07.054.
[28] H.B. Zhou, Y.L. Liu, Y. Zhang, S. Jin, G.H. Lu, First-principles investigation of energetics and site preference of He in a W grain boundary, Nucl. Instrum. Methods Phys. Res. Sect. B 267 (18) (2009) 3189–3192, doi:10.1016/j.nimb.2009.06.067.
[29] H.B. Zhou, Y.L. Liu, S. Jin, Y. Zhang, G.N. Luo, G.H. Lu, Investigating behaviours of hydrogen in a tungsten grain boundary by first principles: from dissolution and diffusion to a trapping mechanism, Nucl. Fusion 50 (2) (2010) 025016, doi:10.1088/0029-5515/50/2/025016.
[30] W.-H. He, X. Gao, D. Wang, N. Gao, M.-H. Cui, L.L. Pang, Z.G. Wang, First-principles investigation of grain boundary morphology effects on helium solutions in tungsten, Comput. Mater. Sci 148 (2018) 224–230, doi:10.1016/j.commatsci.2018.02.044.
[31] U. Saikia, M.B. Sahariah, C. González, R. Pandey, Vacancy assisted he-interstitial clustering and their elemental interaction at fcc-bcc semicoherent metallic interface, Sci. Rep. 8 (1) (2018), doi:10.1038/s41598-018-22141-y.
[32] Y. Yu, X. Shu, Y.-N. Liu, G.-H. Lu, Molecular dynamics simulation of hydrogen dissolution and diffusion in a tungsten grain boundary, J. Nucl. Mater. 455 (1) (2014) 91–95, doi:10.1016/j.jnucmat.2014.04.016. Proceedings of the 16th International Conference on Fusion Reactor Materials (ICFRM-16), URL https://www.sciencedirect.com/science/article/pii/S0022311514002281
[33] U. von Toussaint, S. Gori, A. Manhard, T. Höschen, C. Höschen, Molecular dynamics study of grain boundary diffusion of hydrogen in tungsten, Phys. Scr. T145 (2011) 014036, doi:10.1088/0031-8949/2011/t145/014036.
[34] K.D. Hammond, L. Hu, D. Maroudas, B.D. Wirth, Helium impurity transport on grain boundaries: enhanced or inhibited? EPL (Europhys. Lett.) 110 (5) (2015) 52002, doi:10.1209/0295-5075/110/52002.
[35] C. González, R. Iglesias, Cluster formation and eventual mobility of helium in a tungsten grain boundary, J. Nucl. Mater. 514 (2019) 171–180, doi:10.1016/j.jnucmat.2018.11.029.
[36] R. Gonzalez-Arrabal, A. Rivera, J.M. Perlado, Limitations for tungsten as plasma facing material in the diverse scenarios of the European inertial confinement fusion facility hiPER: current status and new approaches, Matter Radiat. Extremes 5 (5) (2020) 055201, doi:10.1063/5.0010954.
[37] J. Alvarez, A. Rivera, R. Gonzalez-Arrabal, D. Garoz, E. del Rio, J.M. Perlado, Materials research for HiPER laser fusion facilities: chamber wall, structural material and final optics, Fusion Sci. Technol. 60 (2) (2011) 565–569, doi:10.13182/FST11-A12443.
[38] M. Victoria, S. Dudarev, J.L. Boutard, E. Diegele, R. Lässer, A. Almazouzi, M.J. Caturla, C.C. Fu, J. Källne, L. Malerba, K. Nordlund, M. Perlado, M. Rieth, M. Samaras, R. Schaeublin, B.N. Singh, F. Willaime, Modelling irradiation effects in fusion materials, Fusion Eng. Des. 82 (15-24) (2007) 2413–2421, doi:10.1016/j.fusengdes.2007.05.079.
[39] D.M. Duffy, Fusion power: a challenge for materials science, Philos. Trans. R. Soc. A Math. Phys. Eng. Sci. 368 (1923) (2010) 3315–3328, doi:10.1098/rsta.2010.0060.
[40] C.S. Becquart, C. Domain, A density functional theory assessment of the clustering behaviour of He and H in tungsten, J. Nucl. Mater. 386-388 (2009) 109–111, doi:10.1016/j.jnucmat.2008.12.085.
[41] N. Juslin, B.D. Wirth, Molecular dynamics simulation of the effect of subsurface helium bubbles on hydrogen retention in tungsten, J. Nucl. Mater. 438 (2013) S1221–S1223, doi:10.1016/j.jnucmat.2013.01.270.
[42] P. Grigorev, D. Terentyev, G. Bonny, E.E. Zhurkin, G. van Oost, J.-M. Noterdaeme, Mobility of hydrogen-helium clusters in tungsten studied by molecular dynamics, J. Nucl. Mater. 474 (2016) 143–149, doi:10.1016/j.jnucmat.2016.03.022.
[43] S. Markelj, T. Schwarz-Selinger, A. Založnik, Hydrogen isotope accumulation in the helium implantation zone in tungsten, Nucl. Fusion 57 (6) (2017) 064002, doi:10.1088/1741-4326/aa6b27.
[44] Y. Ueda, M. Fukumoto, J. Yoshida, Y. Ohtsuka, R. Akiyoshi, H. Iwakiri, N. Yoshida, Simultaneous irradiation effects of hydrogen and helium ions on tungsten, J. Nucl. Mater. 386–388 (2009) 725–728, doi:10.1016/j.jnucmat.2008.12.300.
[45] V.K. Alimov, B. Tyburska-Püschel, Y. Hatano, J. Roth, K. Isobe, M. Matsuyama, T. Yamanishi, The effect of displacement damage on deuterium retention in ITER-grade tungsten exposed to low-energy, high-flux pure and helium-seeded deuterium plasmas, J. Nucl. Mater. 420 (1–3) (2012) 370–373, doi:10.1016/j.jnucmat.2011.10.025.
[46] O.V. Ogorodnikova, B. Tyburska, V.K. Alimov, K. Ertl, The influence of radiation damage on the plasma-induced deuterium retention in self-implanted tungsten, J. Nucl. Mater. 415 (1) (2011) S661–S666, doi:10.1016/j.jnucmat.2010.12.012.
[47] M. Miyamoto, S. Mikami, H. Nagashima, N. Iijima, D. Nishijima, R.P. Doerner, N. Yoshida, H. Watanabe, Y. Ueda, A. Sagara, Systematic investigation of the formation behavior of helium bubbles in tungsten, J. Nucl. Mater. 463 (2015) 333–336, doi:10.1016/j.jnucmat.2014.10.098.
[48] M.J. Baldwin, R.P. Doerner, W.R. Wampler, D. Nishijima, T. Lynch, M. Miyamoto, Effect of He on D retention in W exposed to low-energy, high-fluence (D, He, Ar) mixture plasmas, Nucl. Fusion 51 (10) (2011) 103021, doi:10.1088/0029-5515/51/10/103021.
[49] G. Kresse, J. Hafner, Ab initio molecular dynamics for liquid metals, Phys. Rev. B 47 (1) (1993) 558–561, doi:10.1103/physrevb.47.558.
[50] G. Kresse, J. Furthmüller, Efficient iterative schemes for ab initio total-energy calculations using a plane-wave basis set, Phys. Rev. B 54 (16) (1996) 11169–11186, doi:10.1103/physrevb.54.11169.
[51] G. Kresse, D. Joubert, From ultrasoft pseudopotentials to the projector augmented-wave method, Phys. Rev. B 59 (3) (1999) 1758–1775, doi:10.1103/physrevb.59.1758.
[52] J.P. Perdew, K. Burke, M. Ernzerhof, Generalized gradient approximation made simple, Phys. Rev. Lett. 77 (18) (1996) 3865–3868, doi:10.1103/physrevlett.77.3865.
[53] P.E. Blöchl, Projector augmented-wave method, Phys. Rev. B 50 (24) (1994) 17953–17979, doi:10.1103/physrevb.50.17953.

[54] H.J. Monkhorst, J.D. Pack, Special points for brillouin-zone integrations, Phys. Rev. B 13 (12) (1976) 5188–5192, doi:10.1103/physrevb.13.5188.
[55] D. Fernández-Pello, J.M. Fernández-Díaz, M.A. Cerdeira, C. González, R. Iglesias, Energetic, electronic and structural DFT analysis of point defects in refractory BCC metals, Mater. Today Commun. 24 (2020) 101323, doi:10.1016/j.mtcomm.2020.101323.
[56] C. González, R. Iglesias, M.J. Demkowicz, Point defect stability in a semicoherent metallic interface, Phys. Rev. B 91 (6) (2015), doi:10.1103/physrevb.91.064103.
[57] C. González, R. Iglesias, Energetic analysis of He and monovacancies in Cu/W metallic interfaces, Mater. Des. 91 (2016) 171–179, doi:10.1016/j.matdes.2015.11.097.
[58] R.F. Bader, Atoms in Molecules: A Quantum Theory, Oxford University Press, 1990.
[59] M. Yu, D.R. Trinkle, Accurate and efficient algorithm for bader charge integration, J. Chem. Phys. 134 (6) (2011) 064111, doi:10.1063/1.3553716.
[60] H. Jónsson, G. Mills, K.W. Jacobsen, Nudged elastic band method for finding minimum energy paths of transitions, 385.
[61] D. Sheppard, R. Terrell, G. Henkelman, Optimization methods for finding minimum energy paths, J. Chem. Phys. 128 (13) (2008) 134106, doi:10.1063/1.2841941.
[62] C.S. Becquart, C. Domain, Ab initio calculations about intrinsic point defects and he in W, Nucl. Instrum. Methods Phys. Res., Sect. B 255 (1) (2007) 23–26, doi:10.1016/j.nimb.2006.11.006.
[63] C.S. Becquart, C. Domain, U. Sarkar, A. DeBacker, M. Hou, Microstructural evolution of irradiated tungsten: ab initio parameterisation of an OKMC model, J. Nucl. Mater. 403 (1–3) (2010) 75–88, doi:10.1016/j.jnucmat.2010.06.003.
[64] K. Heinola, T. Ahlgren, K. Nordlund, J. Keinonen, Hydrogen interaction with point defects in tungsten, Phys. Rev. B 82 (2010) 094102, doi:10.1103/PhysRevB.82.094102.
[65] A. De Backer, D.R. Mason, C. Domain, D. Nguyen-Manh, M.-C. Marinica, L. Ventelon, C.S. Becquart, S.L. Dudarev, Multiscale modelling of the interaction of hydrogen with interstitial defects and dislocations in BCC tungsten, Nucl. Fusion 58 (1) (2017) 016006, doi:10.1088/1741-4326/aa8e0c.
[66] N. Zhang, Y. Zhang, Y. Yang, P. Zhang, Z. Hu, C. Ge, Trapping of helium atom by vacancy in tungsten: a density functional theory study, Eur. Phys. J. B 90 (5) (2017), doi:10.1140/epjb/e2017-80056-1.
[67] Y.-L. Liu, Y. Zhang, H.-B. Zhou, G.-H. Lu, F. Liu, G.-N. Luo, Vacancy trapping mechanism for hydrogen bubble formation in metal, Phys. Rev. B 79 (17) (2009) 172103.
[68] K. Ohsawa, J. Goto, M. Yamakami, M. Yamaguchi, M. Yagi, Trapping of multiple hydrogen atoms in a tungsten monovacancy from first principles, Phys. Rev. B 82 (18) (2010) 184117.
[69] H.-B. Zhou, Y.-L. Liu, S. Jin, Y. Zhang, G.-N. Luo, G.-H. Lu, Towards suppressing H blistering by investigating the physical origin of the H–He interaction in W, Nucl. Fusion 50 (11) (2010) 115010, doi:10.1088/0029-5515/50/11/115010.